Deepdrawability of a round cylindrical cup

Eindhoven University of Technology
Faculty of Mechanical Engineering
Department of Production Engineering and Automation (WPA)

Deepdrawability of a round cylindrical cup

J.A.H. Ramaekers
A. de Winter
M.W.H. Kessels

Maart 1994
WPA rapportnr.: 120007

DEEPDRAWABILITY OF A ROUND CYLINDRICAL CUP

J. A. H. Ramaekers, A. de Winter, M. W. H. Kessels
Section of Production and Automation
Dept of Mechanical Engineering
Eindhoven University of Technology, The Netherlands

Abstract

The deepdrawability of a round cylindrical cup has been studied to find the relationship between the limit drawing ratio LDR and some process parameters. On the basis of upper and lower bound methods of plasticity, the models necessary to calculate the actual and critical deepdrawing forces have been developed. From the results calculated, the relation between the LDR and process parameters can be derived. The findings agree well with experimental results and general knowledge in practice.

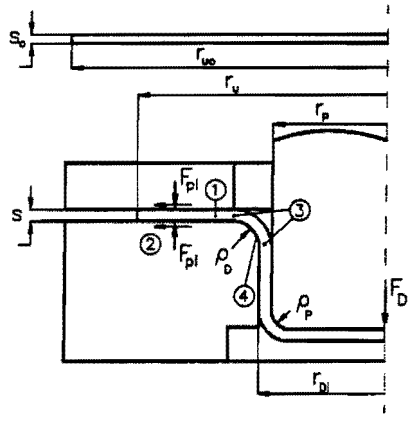

Figure 1: Deepdrawing of a cup

1 Introduction

The relationship between deepdrawability and material propertities, such as strain hardening exponent n and anisotropy factor R, is one of the key factors in sheet metal forming.

In the present work this relation has been studied via the the modelling of the deepdrawing of a round cylindrical cup. As a measure of deepdrawability, the limit drawing ratio LDR is widely used. The LDR or β_{0max}, is the drawing ratio where the maximum deepdrawing force F_{Dmax} equals the strength of the cup in the punch-nose region, the critical force F_C, upon which a fracture will occur in the weakest zone of the cup and the operation that follows will fail.

Based on the upper and lower bound methods, theoretical models for F_{Dmax} and F_C have been developed, which are in good agreement compared with the experimental ones. Application of the criterion, $F_{Dmax} = F_C$, gives us the LDR in relation with material properties (n, R), friction (μ), blankholder force and tool geometry (ρ_P, ρ_D, r_P). (see Fig. 1)

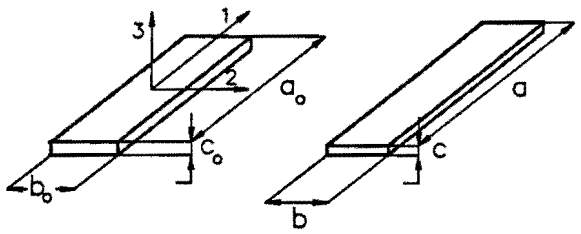

Figure 2: Deformation model

2 Basic Formulations

The approach presented in this paper is based on following assumptions:

1. The deformation can be described by finite principal strains:

$$\epsilon_1 = \ln \frac{a}{a_0}, \ \epsilon_2 = \ln \frac{b}{b_0}, \ \epsilon_3 = \ln \frac{c}{c_0} \quad (1)$$

where a_0, b_0, c_0 and a, b, c are the dimensions of a rectangular element before and after deformation.(see Fig. 2)

2. The normal stress of the sheet surface is negligible compared to other principal stresses σ_1 and σ_2. Therefore the plane stress condition is assumed $\sigma_3 = 0$

3. The anisotropic behavior is sufficiently described by

$$R_\alpha = (\frac{\epsilon_2}{\epsilon_3})_\alpha, \quad (\sigma_2 = \sigma_3 = 0) \quad (2)$$

where α is angle to the roll direction, and

$$R = \frac{1}{4}(R_0 + R_{90} + 2R_{45}) \quad (3)$$

4. The effective strain is defined as:

$$\bar{\epsilon} = \sqrt{\frac{R+1}{2R+1}(\epsilon_1^2 + \epsilon_2^2 + R\epsilon_3^2)} \quad (4)$$

5. The effective stress is defined as:

$$\bar{\sigma} = \sqrt{\sigma_1^2 - \frac{2R}{R+1}\sigma_1\sigma_2 + \sigma_2^2} \quad (5)$$

6. Strain hardening behavior

$$\sigma_f = C(\bar{\epsilon} + \epsilon_0)^n \quad (6)$$

7. Yielding criterion

$$\bar{\sigma} = \sigma_f \quad (7)$$

8. Friction law

$$F_{Fr} = \mu F_N \quad or \quad \tau_{Fr} = \mu\sigma_3 \quad (8)$$

3 The Deepdrawing Force F_D^*

In the deepdrawing process, four factors contribute to the energy dissipation, which are:

- F_{Dfl} - Deformation of the flange
- $F_{D\rho}$ - Bending of the sheet at die radius
- F_{Frfl} - Friction between the tool and flange
- $F_{Fr\rho}$ - Friction at the die radius

Introducing the dimensionless quantities, we have

$$F^* = \frac{F}{2\pi r_p s_0 C} = P^* = \frac{P}{2\pi r_p s_0 C\dot{u}} \quad (9)$$

where P is power, F is force and $\dot{u}$ is punch velocity. Applying the virtual work theorem, it yields:

$$F_D^* = F_{Dfl}^* + F_{D\rho}^* + F_{Frfl}^* + F_{Fr\rho}^* \quad (10)$$

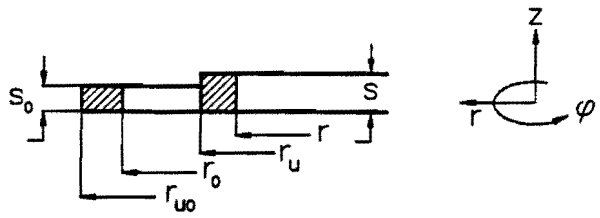

Figure 3: The flange deformation

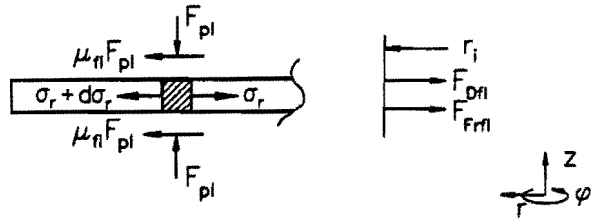

Figure 4: Forces on the flange

3.1 The Flange Deformation

Assuming the normal of the flange remains unchanged during the process

$$s = s(r_u/r_{u0}) \neq s(r) \tag{11}$$

and using invariance of volume (see Fig. 3), it yields:

$$(r_{u0}^2 - r_0^2)s_0 = (r_u^2 - r^2)s \tag{12}$$

therefore, strains can be derived as:

$$\begin{aligned} \epsilon_\phi &= -\frac{1}{2}\ln\{(\frac{r_{u0}}{r})^2 \\ &- ((\frac{r_u}{r})^2 - 1)\frac{s}{s_0}\} \\ \epsilon_z &= \ln\frac{s}{s_0},\ \epsilon_r = -(\epsilon_\phi + \epsilon_z) \end{aligned} \tag{13}$$

At the edge of the flange ($r = r_u$) it holds that $\sigma_r = \sigma_z = 0$. Using equation 2 we get:

$$\frac{\epsilon_\phi}{\epsilon_{z\,(r=r_u)}} = -(R+1) \tag{14}$$

which gives

$$\frac{s}{s_0} = (\frac{r_{u0}}{r_u})^{\frac{1}{R+1}} \tag{15}$$

The effective strain and stress can now be calculated with equations (3, 4, 5, 13, 15)

3.2 The Stresses in the Flange

Using the slab method (see Fig. 4), the differential equation can be derived as:

$$d\sigma_r + (\sigma_r - \sigma_\phi)\frac{dr}{r} = 0 \tag{16}$$

Adopting the modified Tresca yielding criterion, it yields:

$$\sigma_r - \sigma_\phi = K_f\sigma_{f(r)} \tag{17}$$

with $K_f = 1.06 - 0.015R$.
The yielding stress over the flange can be interpolated as:

$$\sigma_{f(r)} = \sigma_{fu} - (\sigma_{fi} - \sigma_{fu})\frac{r_u - r}{r_u - r_i} \tag{18}$$

where $\sigma_{fu} = \sigma_{f(r=r_u)}$, $\sigma_{fi} = \sigma_{f(r=r_i)}$, $r_i = \frac{1}{2}(r_P + r_{Di})$

And solution of the differential equation gives:

$$\begin{aligned} \sigma_r(r) &= K_f\sigma_{fu}[(1 + \frac{K_\sigma - 1}{1 - \frac{r_i}{r_u}})\ln\frac{r_u}{r} \\ &-(K_\sigma - 1)\frac{r_u - r}{r_u - r_i}] \end{aligned} \tag{19}$$

where $K_\sigma = \sigma_{fi}/\sigma_{fu}$

3.3 The Flange Force F^*_{Dfl}

With equation

$$F^*_{Dfl} = \frac{r_i}{r_P C}\frac{s}{s_0}\sigma_{r(r=r_i)} \qquad (20)$$

The contribution of the deformation of the flange can be calculated as:

$$F^*_{Dfl} = K_f(\ln\frac{\beta_0}{\beta} + \epsilon_0)^n(\frac{\beta_0}{\beta})^{\frac{1}{R+1}} \qquad (21)$$
$$\{1 - K_\sigma + (1 + \frac{K_\sigma - 1}{1 - 1/\beta})\ln\beta\}(1 + \frac{s_0}{2r_P})$$

where $\beta_0 = r_{u0}/r_i, \quad \beta = r_u/r_i$

3.4 The Bending Effect $F^*_{D\rho}$

The bending and re-bending of the sheet at the die radius is considered to be a stationary process. The contribution to the total deformation power can be calculated as:

$$F^*_{D\rho} = \frac{r_i}{r_P}\frac{s}{s_0}\frac{\sigma_{fi}}{C}\Delta\bar{\epsilon}_b \qquad (22)$$

where $\Delta\bar{\epsilon}_b$ is the average increase of the effective strain due to the bending, and is defined as:

$$\Delta\bar{\epsilon}_b \approx \frac{1}{1 + 2\rho_D/s}\frac{R+1}{\sqrt{2R+1}} \qquad (23)$$

Using equation 22 and 23 we find:

$$F^*_{D\rho} = K_\rho\frac{\sigma_{fi}}{C}\frac{R+1}{\sqrt{2R+1}} \qquad (24)$$
$$\frac{s}{2\rho_D + s}(1 + \frac{s_0}{2r_P})$$

The factor K_ρ is the correction factor. A comparison with experimental results gives $K_\rho \approx 0.8$

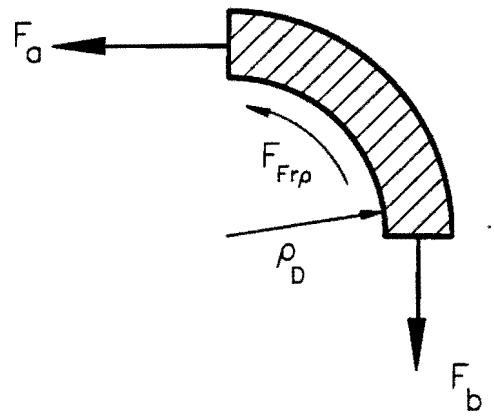

Figure 5: Forces at die radius

3.5 The Friction Between Flange and Tool F^*_{Frfl}

Equilibrium of forces on the flange gives:

$$F^*_{Frfl} = \mu_{fl}\frac{r_P}{s_0}\frac{P_{blh}}{C}\{(\frac{r_{u0}}{r_P})^2 - (\frac{r_{Di}+\rho_D}{r_P})^2\} \qquad (25)$$

with P_{blh}, the bankholder pressure according to Siebel [1]:

$$P_{blh} = 0.00225\{(\beta_0 - 1)^2 + 0.01\beta_0\frac{r_P}{s_0}\}C(\frac{n}{e})^n e^{\epsilon_0} \qquad (26)$$

3.6 The Friction at Die Radius $F^*_{Fr\rho}$

Sniekers [2] [3] has shown that the so-called rope formula

$$F_b = F_a e^{\mu\pi/2} \qquad (27)$$

is invalid in application to the friction at die radius, because of the bending stiffness of the sheet. As an approximation. the following is applied:

$$F^*_{Fr\rho} = 1.6\mu_\rho F^*_a \qquad (28)$$

with $F^*_a = F^*_{Dfl} + F^*_{Frfl} + \frac{1}{2}F^*_{D\rho}$

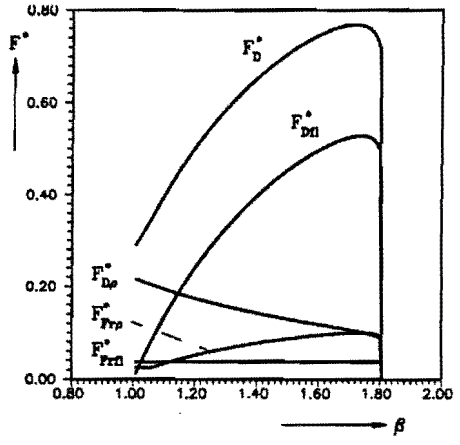

Figure 6: Components of the deepdrawing force of Aluminum: $F^*_{Dfl}, F^*_{D\rho}, F^*_{Frfl}, F^*_{Fr\rho}$

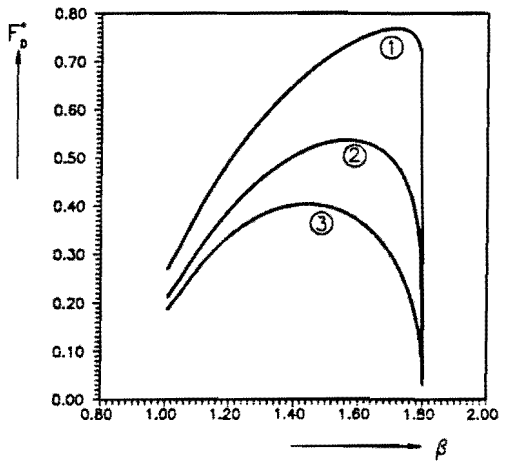

Figure 7: The deepdrawing force of three materials: 1) Aluminum, 2) C-Steel, 3) Stainless Steel

3.7 The Deepdrawing Force F^*_D, F^*_{Dmax}

With the formula derived the force-path diagram is calculated for three different materials (see Fig. 6 and Fig. 7) under following the conditions: $\mu_\rho = 2\mu_{fl} = 0.1, r_P/s_0 = 100, \rho_D/s_0 = 4, \beta_0 = 1.8$

C-Steel: $n = 0.25, \quad \epsilon_0 = 0, \quad R = 1.65$
Alu-Hard: $n = 0.05, \quad \epsilon_0 = 0, \quad R = 0.65$
Stain-Steel: $n = 0.5, \quad \epsilon_0 = 0, \quad R = 1$

From the force-path diagram calculated, the maximum force can be extracted. Fig. 8 gives the maximum deepdrawing force as a function of the strain hardening exponent n. The experimental measurements, which are also shown in the figure, are normalised to $\beta_0 = 2, \rho_D/s_0 = 4$. With correction:

$$F^*_{Dmaxexp} = \frac{F_{Dexp}}{2\pi r_P s_0 C} \frac{1}{\beta_0 - 1} + 0.02\left(\frac{\rho_D}{s_0} - 4\right) \quad (29)$$

Some conclusions can be drawn from the measurements and calculations:

1. The agreement between theory and experiments is quite satisfying.

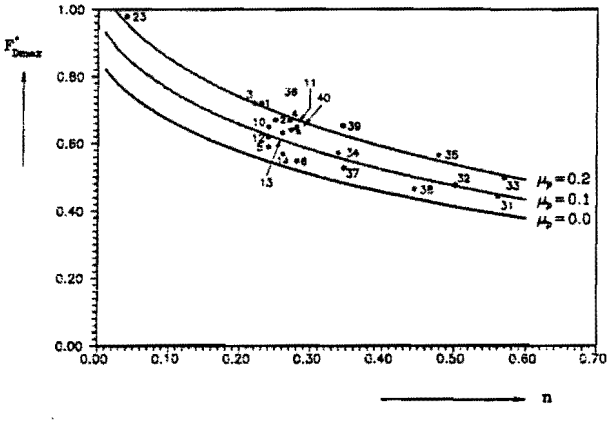

Figure 8: The maximum deepdrawing force vs strain hardening exponent n, with $\rho_D/s_0 = 4, \epsilon_0 = 0, R = 1, \beta_0 = 2$ for different materials

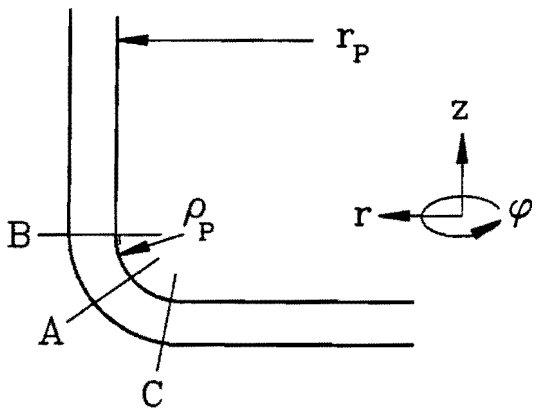

Figure 9: Three different failure types

2. An optimal die radius $\rho_{Dopt} \approx 4 - 6s_0$.
3. The anisotropy factor R has minor influence on the deepdrawing force.
4. The pre-strain has no influence on the deepdrawing force, since in most cases the pre-strain is very small ($\epsilon_0 < 0.01$).
5. The maximum deepdrawing force is a linear function of β_0.

$$F_D^* = F_{Dmax(\beta_0=2)}^*(\beta_0 - 1) \qquad (30)$$

6. As the size of products increases, the influence of the flange friction increases. In car body production, lubrication and friction in particular are major factors.

4 The Critical Force

Doege [4] has pointed out three possible failure types:

1. Type A: Fracture in the corner zone, which is considered to be the normal one.
2. Type B: Fracture in the straight wall of the cup outside the corner zone. This gives higher values of the critical force, and thus higher LDR. However, the conditions under which this optimal failure type occurs are uncertain.
3. Type C: Failure in the bottom zone, as indicated by Oehler as preamble fracture. This type of failure should be avoided by improving the process parameters.

The critical force related to the failure type B can easily be deduced. In the wall of the cup we know: $\sigma_r = \epsilon_\phi = 0$, therefore:

$$\sigma_f = \sigma_z \frac{\sqrt{2R+1}}{R+1} \qquad (31)$$

$$\bar{\epsilon} = \frac{R+1}{\sqrt{2R+1}} \ln \frac{s_0}{s} \qquad (32)$$

The dimesionless maximum force in the wall of cup can be derived as:

$$F_{CB}^* = \left(\frac{R+1}{\sqrt{2R+1}}\right)^{n+1} \left(\frac{n}{e}\right)^n e^{\frac{\sqrt{2R+1}}{R+1}\epsilon_0} \qquad (33)$$

Kals [5] derived a model for the failure type A. This model is corrected for the influence of the anisotropy factor R as follows:

$$F_{CA}^* = \frac{\left(\frac{R+1}{\sqrt{2R+1}}\right)^{n+1} n^n}{\left(\frac{s_0}{\rho_P} + \frac{s_0}{r_P} + e^{n - \frac{\sqrt{2R+1}}{R+1}\epsilon_0}\right)} \qquad (34)$$

Fig. 10 gives the results of calculations and measurements. in which the experimental values are corrected for $R = 1$ with

$$F_{Cexp}^* = \frac{F_{Cexp}}{2\pi r_P s_0 C} \left(\frac{2\sqrt{2R+1}}{(R+1)\sqrt{3}}\right)^{n+1} \qquad (35)$$

Some conclusions concerning the critical force can be drawn:

1. The agreement between the experiment and theory is satisfying.

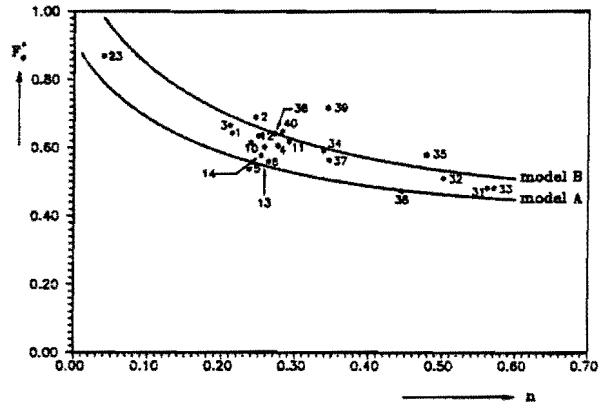

Figure 10: The critical force F_C^*

2. The optimal die radius with respect to the strength of the punch-nose zone and the risk of wrinkling is: $\rho_{opt} \approx 4 - 6s_0$.
3. In practice, it is recommended that formula 34 is used to conclude the deepdrawability.
4. The anisotropy factor R has a major influence on the critical force.
5. In most cases ($\epsilon_0 < 0.01$) the pre-strain has little influence on the critical force.
6. The friction between punch and cup wall can have a positive influence on the load in the critical zone. In practice, this can be used to reach very high LDR values [6]. In the current work, this influence is not investigated.

5 Limit Drawing Ratio LDR

The LDR can be derived with $F_{Dmax}^* = F_C^*$ [7]. Fig. 11 gives a schematic way to find the relation between β_{0max} and the process parameters. Fig. (12, 13, 14, 15) show F_{Dmax}^* against LDR with n and R as parameters for different product sizes under the condition of $\mu_P = 2\mu_{fl} = 0.1$ and $\rho_P = \rho_D = 4s_0$

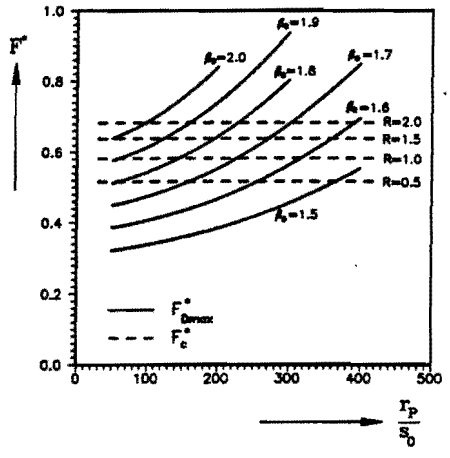

Figure 11: The deepdrawing force vs process parameters with $n = 0.25, \rho_P = \rho_D = 4s_0$

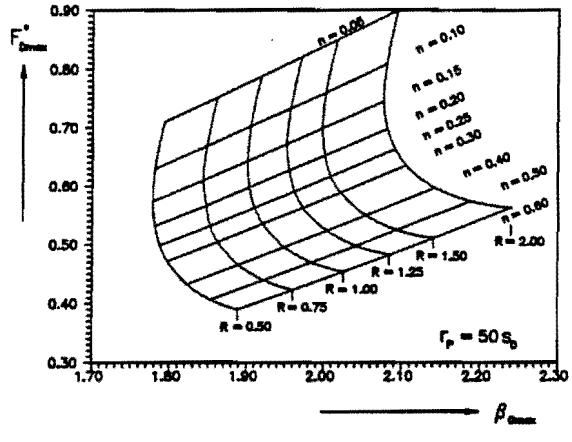

Figure 12: F_{Dmax}^* vs LDR with n and R as parameters

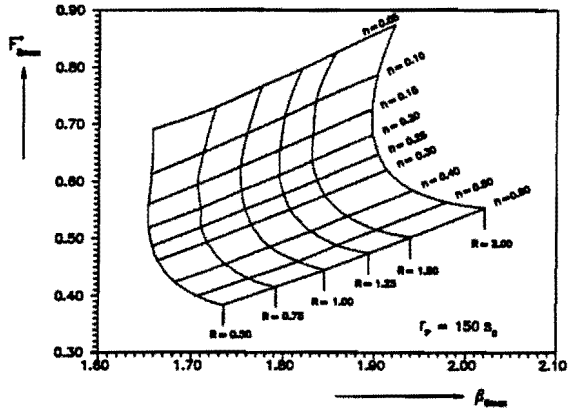

Figure 13: F^*_{Dmax} vs LDR with n and R as parameters

Fig. (16, 17) show LDR as a function of the product size with friction coefficient μ_P and μ_{fl} as parameters. The calculated values are compared with emperical findings of the TNO Laboratory. The TNO Lab. data do not distinguish the difference of different materials. Fig. 18 shows the influence of the anisotropy factor R on the deepdrawability with $n = 0.25$.

6 Conclusions

From the results of the calculations compared with empirical data and general knowledge in practice, the following conclusions can be drawn:

1. There is good agreement between our model and the experimental results.
2. Due to the scatteredness of input data, the LDR can not be predicted very precisely.
3. General conclusions on deepdrawability of materials can be extracted from the graphs designed. These conclusions agree well with practical experience.

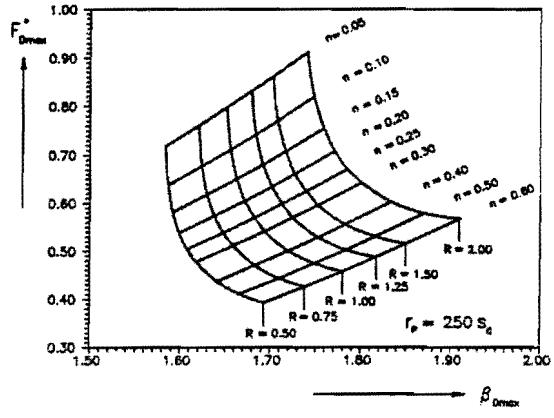

Figure 14: F^*_{Dmax} vs LDR with n and R as parameters

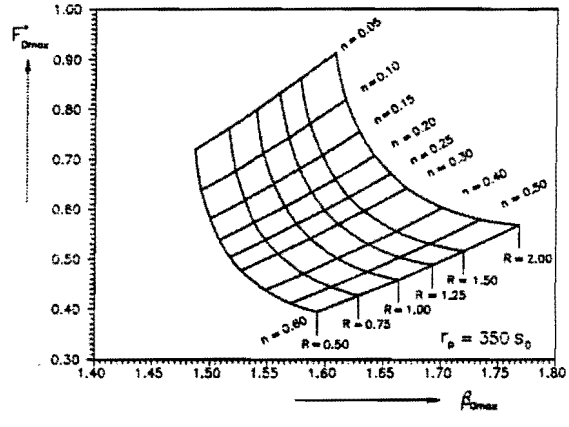

Figure 15: F^*_{Dmax} vs LDR with n and R as parameters

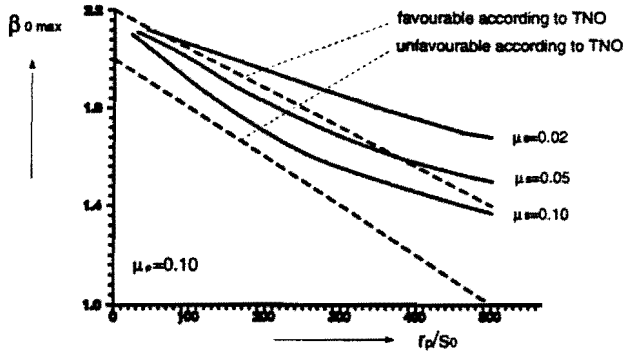

Figure 16: LDR vs product size with collected experimental data from the TNO Lab, under the condition $\mu_P = 0.1, n = 0.25, R = 1.8$

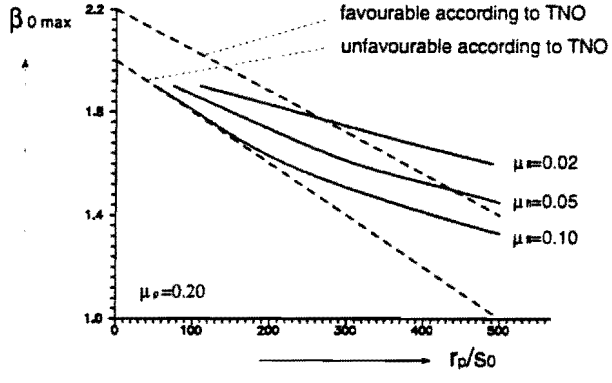

Figure 17: LDR vs product size with collected experimental data from the TNO Lab, under the condition $\mu_P = 0.2, n = 0.25, R = 1.8$

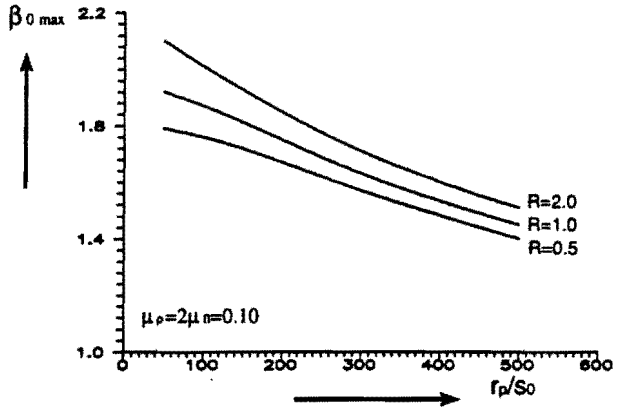

Figure 18: The influence of R on LDR

4. Besides parameters like ρ_P and ρ_D, the friction factor μ is of vital importance for the deepdrawability of large-size products. This is one of the most interesting subjects for future research.

5. Although the process speed was not the subject of the present research, some remarks can still be made:
   For materials which are strainrate sensitive, F_D will increase while F_C remains constant, so a negative influence on the LDR will occur. For a large product, friction is of more influence on LDR. Generally, decreasing μ will increase LDR. An investigation of the influence of the press speed on LDR is worth while.

6. Also less attention is given to the influence of the blankholder force on LDR. This influence can be deduced from the theoretical modelling. It is worthwhile to investigate the possible benefits of a flexible blankholder force.

7. The information from the literature concerning the blankholder force is not unequivocal. One of the suggested for-

mula is used in our calcualtions. Generally, re-calculation with the real value of the blankholder force is necessary, especially for large products.

Acknowledgments

The authors wishes to thank the Dutch governmental institution IOP-M for its support of this research.

References

[1] Siebel, E. 'Der Niederhalterdruck beim Tiefziehen', Stahl und Eisen, nr.3 (jrg.74) 28 jan. 1954, blz.155-158

[2] Sniekers, R. J. J. M., Ramaekers, J. A. H. 'Experiments on stripdrawing with stationary bending and strainhardening', Proc. 4th ICTP, Beijing, 1993. page 1716

[3] Hoogenboom, S. M., Sniekers, R. J. J. M., 'Analysis of stationary bending and strainhardening during stripdrawing', Proc. 4th ICTP, Beijing, 1993. page 1722

[4] Doege, E. 'Untersuchungen über die maximal übertragbare Stempelkraft beim Tiefziehen rotationssymmetrische zylindrische Teile'. Ingenieur Dissertation TU Berlin 1963

[5] Kals, J. A. G., 'Der Einfluss der Stempelgeometrie auf die kritische Tiefziehkraft', Annals of CIRP 19 (1970) page 291-296

[6] Pischel, H. 'Das hydromechanische Ziehverfahren'. Mitteilungen DFBO, 1970, nr.1 pag. 15-19

[7] de Winter, A., 'Modellen en analyse het dieptrekken van ronde produkten', TUE-research report WPA 1470

[8] Ramaekers, J.A.H., Houtackers, L.J.A., Peeters, P.B.G.,'Plastisch bewerken van metalen', Mierlo, Omtec 1989

[9] Ramaekers, J.A.H., Kessels, M.W.H., 'Een plastisch model voor het dieptrekproces', TUE-research report WPA 1572